Progress In Electromagnetics Research Letters, Vol. 92, 93–100, 2020

Four Dimensional Strictly Noncircular Unitary ESPRIT Algorithm for L-Shaped Bistatic MIMO Radar

Yonghong Liu[1, 2], Jiaxiong Fang[1], Tianyi Zhao[1], Hua Chen[1, 2], and Weiyue Liu[1, *]

Abstract—In this paper, a joint two dimensional (2D) direction of departure (DOD) and 2D direction of arrival (DOA) strictly noncircular (NC) unitary estimation of signal parameters via rotational invariance techniques (ESPRIT) method is proposed for an L-shaped bistatic multiple input multiple output (MIMO) radar. In the case that the incident signals are NC signals, we first utilize the received data vector and its conjugate counterparts to construct a new data vector, and then the unitary ESPRIT method is adopted to estimate the 2D-DODs and 2D-DOAs, which can automatically pair the four dimensional (4D) angle parameters. Simulation results are included to verify the effectiveness of the proposed algorithm.

1. INTRODUCTION

As a new type of radar system, multiple input multiple output (MIMO) radar has many potential advantages in enhancing spatial resolution, parameter identification, and improving target detection capability [1, 2]. In MIMO radar, angle estimation is an important issue that has drawn significant attention in recent years [3, 4]. For a MIMO radar system deployed with uniform linear arrays (ULAs), the problem of joint direction of departure (DOD) and direction of arrival (DOA) [5–7] estimation is studied, which is based on excellent two dimensional (2D)-DOA estimation methods such as the multi-signal classification (MUSIC) method [8], estimation of signal parameters via rotational invariance techniques (ESPRIT)-based methods [9–11], the method of combining ESPRIT and MUSIC [12], and the method proposed in the presence of unknown mutual coupling [13]. In [14, 15], joint estimation of 2D-DOD and 2D-DOA is presented by transforming the four dimensional (4D) angle estimates into four one dimensional (1D) estimates for bistatic MIMO radar deployed with plane arrays. However, none of the above work considers the noncircularity characteristics of the signal.

With the aid of the noncircularity characteristic of noncircular (NC) signals [16, 17], a series of angle estimation methods [18–20] for bistatic MIMO radar are proposed, which can improve the accuracy of angle estimation and detect more signals. In [18], the combined ESPRIT and MUSIC approach was applied to a bistatic MIMO radar in the case of NC incoming signals, but its computational complexity was still relatively high. To solve this problem, in [19], the authors proposed an ESPRIT-based method which is appropriate for the coexistence of noncircular and circular signals in bistatic MIMO radar. In [20], a low complexity real value ESPRIT algorithm for NC signals was proposed with real-value computation. However, the problem of 2D-DOD and 2D-DOA estimation using noncircularity characteristic has been rarely reported so far. Therefore, by exploiting the noncircular property of transmitting signals, this paper proposes a 4D NC Unitary ESPRIT algorithm to estimate 2D-DOD and 2D-DOA for an L-shaped bistatic MIMO radar. The main contributions of the proposed method are as follows:

Received 24 May 2020, Accepted 23 June 2020, Scheduled 4 July 2020

* Corresponding author: Weiyue Liu (liuweiyue@nbu.edu.cn).

[1] Faculty of Electrical Engineering and Computer Science, Ningbo University, Ningbo 315211, China. [2] Key Laboratory of Intelligent Perception and Advanced Control of State Ethnic Affairs Commission, Dalian 116600, China.

(1) A non-circular array signal model based on an L-shaped bistatic MIMO radar is constructed.
(2) The proposed algorithm can work in the case of common 1D DOD and DOA, and automatically pair the 4D angle parameters.
(3) The algorithm derives the closed-form stochastic Cramer-Rao bound (CRB) expression as a performance benchmark.

The rest of this article is organized as follows. Section 2 introduces the signal model. The proposed algorithm is described in Section 3. Also the Cramer-Rao Bound for the considered scenario is derived in Section 4. The experimental simulation results are conducted in Section 5. Finally, Section 6 draws the conclusion.

Notations: $(\cdot)^*$, $(\cdot)^T$, $(\cdot)^+$, and $(\cdot)^H$ denote conjugate, transpose, pseudo-inverse, and conjugate transpose, respectively. diag$(\cdot)$ denotes the diagonal matrix; blkdiag$(\cdot)$ represents the generation of a block diagonal matrix; $\otimes$ and $\odot$ are the Kronecker and Hadamard product, respectively; $\mathbf{I}_k$ denotes the k-dimensional identity matrix; $\mathbf{\Upsilon}_k$ denotes the k-dimensional exchange matrix; $\mathbf{0}_{k\times l}$ denotes the $k \times l$ zero matrix; arg$(\cdot)$ is the phase operation.

2. SIGNAL MODEL

Consider a bistatic MIMO radar system with an L-shaped transmit antenna array for transmitting and an L-shaped receive antenna array for receiving, as shown in Fig. 1. The transmitting array has a total number of $M = M_1 + M_2 - 1$ antennas, with M_1 and M_2 antennas located on the X and Y axes, respectively, and the receiving array has $N = N_1 + N_2 - 1$ antennas, of which N_1 and N_2 elements are located on the X' and Y' axes, respectively. The four subarrays are all uniform linear arrays (ULAs) with the antennas to be omnidirectional and interelement spaced d that equals half-wavelength. It is assumed that the reflection coefficient caused by the Doppler frequency to the signal can be ignored. The transmitted waveforms are M orthogonal BPSK modulated signals. The targets are the far field signals related to the transmitting and receiving arrays with directions parameterized as $(\theta_{k1}, \theta_{k2}, \theta_{k3}, \theta_{k4})$, where $(\theta_{k1}, \theta_{k2})$ is the 2D-DOD of the kth target, and $(\theta_{k3}, \theta_{k4})$ is the 2D-DOA. Thus, the output of the entire matched filters at the receiving array at time t can be expressed as

$$\mathbf{X}(t) = \mathbf{C}(\theta_{k1}, \theta_{k2}, \theta_{k3}, \theta_{k4})\mathbf{S}(t) + \mathbf{N}(t) \tag{1}$$

where $\mathbf{X}(t) = [\mathbf{x}_1(t), \cdots, \mathbf{x}_{MN}(t)]^{\mathrm{T}}$ is the $MN \times L$ data matrix, and L is the number of snapshots. $\mathbf{C} = [\mathbf{c}_1, \cdots, \mathbf{c}_K]^{\mathrm{T}}$ is the $MN \times K$ extended virtual array manifold matrix; $\mathbf{c}_k = \mathbf{b}_k \otimes \mathbf{a}_k$ is the $MN \times 1$ extended virtual array manifold vector; $\mathbf{a}_k$ and $\mathbf{b}_k$ are the $M \times 1$ transmitting and $N \times 1$ receiving array manifold vectors, which has the form of $\mathbf{a}_k = [e^{j2\pi\lambda^{-1}dM_2\cos\theta_{k2}}, \cdots, 1, \cdots, e^{j2\pi\lambda^{-1}dM_1\cos\theta_{k1}}]^{\mathrm{T}}$ and $\mathbf{b}_k = [e^{j2\pi\lambda^{-1}dN_2\cos\theta_{k4}}, \cdots, 1, \cdots, e^{j2\pi\lambda^{-1}dN_1\cos\theta_{k3}}]^{\mathrm{T}}$, respectively. $\mathbf{N}(t) = [\mathbf{n}_1(t), \cdots, \mathbf{n}_{MN}(t)]^{\mathrm{T}}$

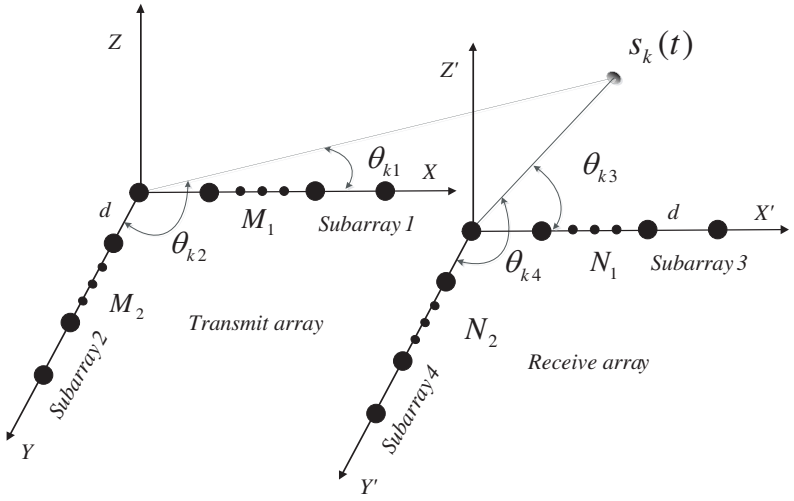

Figure 1. An L-shaped MIMO array structure.

is the $MN \times L$ additive white Gaussian noise matrix with zero mean and variance σ_n^2. $\mathbf{S}(t) = [\mathbf{s}_1(t), \cdots, \mathbf{s}_K(t)]^{\mathrm{T}}$ is the $K \times L$ matrix, where $\mathbf{s}_k(t) = e^{j\varphi_k} \cdot \beta_k e^{j2\pi f_k t}\mathbf{r}_k(t)$, $\mathbf{r}_k(t)$ is the NC signal vector; φ_k is the noncircular phase of the kth NC signal; β_k and f_k represent the refection coefficients and Doppler frequencies of the kth target, respectively.

Then, $\mathbf{s}_k(t)$ can be rewritten as $\mathbf{s}_k(t) = e^{j\varphi_k}\tilde{\mathbf{r}}_k(t)$, where $\tilde{\mathbf{r}}_k(t) = \beta_k e^{j2\pi f_k t}\mathbf{r}_k(t)$. Thus, $\mathbf{S}(t)$ can be rewritten as

$$\mathbf{S}(t) = \mathbf{\Phi}\tilde{\mathbf{S}}(t) \tag{2}$$

where $\mathbf{\Phi} = \mathrm{diag}(e^{j\varphi_1}, \cdots, e^{j\varphi_K})$ and $\tilde{\mathbf{S}}(t) = [\tilde{\mathbf{r}}_1(t), \cdots, \tilde{\mathbf{r}}_K(t)]^{\mathrm{T}}$. According to Eqs. (1) and (2), the data matrix is given by

$$\mathbf{X}(t) = \mathbf{C}\mathbf{\Phi}\tilde{\mathbf{S}}(t) + \mathbf{N}(t) \tag{3}$$

For notional convenience, the time t and angle pair $(\theta_{k1}, \theta_{k2}, \theta_{k3}, \theta_{k4})$ will be omitted in the following sections.

3. THE PROPOSED ALGORITHM

In order to utilize the noncircularity characteristic of the NC signals, a new data matrix $\mathbf{Y}$ is defined by stacking the original data matrix $\mathbf{X}$ and its corresponding conjugate counterparts as

$$\begin{aligned}\mathbf{Y} &= \begin{bmatrix} \mathbf{X} \\ \mathbf{\Upsilon}_{MN}\mathbf{X}^* \end{bmatrix} \\ &= \begin{bmatrix} \mathbf{C}\mathbf{\Phi}\tilde{\mathbf{S}} \\ \mathbf{\Upsilon}_{MN}\mathbf{C}^*\mathbf{\Phi}^*\tilde{\mathbf{S}}^* \end{bmatrix} + \begin{bmatrix} \mathbf{N} \\ \mathbf{\Upsilon}_{MN}\mathbf{N} \end{bmatrix} \\ &= \tilde{\mathbf{C}}\tilde{\mathbf{S}} + \tilde{\mathbf{N}}\end{aligned} \tag{4}$$

where $\tilde{\mathbf{C}} = \begin{bmatrix} \mathbf{C}\mathbf{\Phi} \\ \mathbf{\Upsilon}_{MN}\mathbf{C}\mathbf{\Phi} \end{bmatrix}$ is the $2MN \times K$ extended array manifold matrix, and $\tilde{\mathbf{N}} = \begin{bmatrix} \mathbf{N} \\ \mathbf{\Upsilon}_{MN}\mathbf{N} \end{bmatrix}$ is the $2MN \times L$ noise matrix, and $\tilde{\mathbf{S}} = \tilde{\mathbf{S}}^*$.

As pointed in [20], due to real-valued processing, the corresponding method can reduce the computational complexity. Therefore, in the first step of NC unitary ESPRIT, we extend the new data matrix $\mathbf{Y}$ to $\tilde{\mathbf{Y}} = [\ \mathbf{Y} \quad \mathbf{Y}\mathbf{\Upsilon}_L\ ]$. Then, transform complex-valued extended data matrix into the $2MN \times 2L$ real-valued matrix [11]

$$\mathbf{Z} = \mathbf{Q}_{2MN}^H[\ \mathbf{Y} \quad \mathbf{Y}\mathbf{\Upsilon}_L\ ]\mathbf{Q}_{2L}^H \tag{5}$$

where $\mathbf{Q}_P$ is the unitary matrix defined as

$$\begin{aligned}\mathbf{Q}_{2P} &= \frac{1}{\sqrt{2}}\begin{bmatrix} \mathbf{I}_P & j\mathbf{I}_P \\ \mathbf{\Upsilon}_P & -j\mathbf{\Upsilon}_P \end{bmatrix} \\ \mathbf{Q}_{2P+1} &= \frac{1}{\sqrt{2}}\begin{bmatrix} \mathbf{I}_P & \mathbf{0}_{P\times 1} & j\mathbf{I}_P \\ \mathbf{0}_{1\times P} & \sqrt{2} & \mathbf{0}_{1\times P} \\ \mathbf{\Upsilon}_P & \mathbf{0}_{P\times 1} & -j\mathbf{\Upsilon}_P \end{bmatrix}\end{aligned} \tag{6}$$

Performing singular value decomposition (SVD) on the real-valued matrix $\mathbf{Z}$, we can get

$$\mathbf{Z} = \mathbf{U}_S\mathbf{\Sigma}_S\mathbf{V}_S^H + \mathbf{N}_N\mathbf{\Sigma}_N\mathbf{V}_N^H \tag{7}$$

where $2MN \times K$ matrix $\mathbf{U}_S$ and $2L \times K$ matrix $\mathbf{V}_S$ are the left and right singular signal subspaces associated with corresponding left and right singular values matrices $\mathbf{\Sigma}_S$ and $\mathbf{\Sigma}_N$, respectively, while $2MN \times (2MN - K)$ matrix $\mathbf{U}_N$ and $2L \times (2MN - K)$ matrix $\mathbf{U}_N$ are the left and right singular noise subspaces, respectively.

Define a new matrix $\mathbf{E}_S$ as $\mathbf{E}_S = \mathbf{E}_S\mathbf{\Sigma}_S$, and the following selection matrices

$$\mathbf{J}_{1a} = [\ \mathbf{0}_{(a-1)\times(M-a)} \quad \mathbf{0}_{(a-1)\times 1} \quad \mathbf{I}_{a-1}\ ] \tag{8}$$

$$\mathbf{J}_{2a} = [\ \mathbf{0}_{(a-1)\times(M-a)} \quad \mathbf{I}_{a-1} \quad \mathbf{0}_{(a-1)\times 1}\ ] \tag{9}$$

$$\mathbf{J}_{1b} = [\ \mathbf{I}_{b-1} \quad \mathbf{0}_{(b-1)\times 1} \quad \mathbf{0}_{(b-1)\times(M-b)}\ ] \tag{10}$$

$$\mathbf{J}_{2b} = [\ \mathbf{0}_{(b-1)\times 1} \quad \mathbf{I}_{b-1} \quad \mathbf{0}_{(b-1)\times(M-b)}\ ] \tag{11}$$

where $a = M_1, N_1$ and $b = M_2, N_2$. The selection matrices for $\theta_{kl}(l = 1, 2)$ of the NC signals can be expressed as

$$\mathbf{K}_{l1} = \text{blkdiag}\left(\mathbf{J}_{l1}, \mathbf{\Upsilon}_{(M_l-1)M}\mathbf{J}_{l2}\mathbf{\Upsilon}_{MN}\right), l = 1, 2 \tag{12}$$

$$\mathbf{K}_{l2} = \text{blkdiag}\left(\mathbf{J}_{l2}, \mathbf{\Upsilon}_{(M_l-1)M}\mathbf{J}_{l1}\mathbf{\Upsilon}_{MN}\right), l = 1, 2 \tag{13}$$

where $\mathbf{J}_{11} = \mathbf{I}_M \otimes \mathbf{J}_{1M_1}$, $\mathbf{J}_{12} = \mathbf{I}_M \otimes \mathbf{J}_{2M_1}$, $\mathbf{J}_{21} = \mathbf{I}_M \otimes \mathbf{J}_{1M_2}$ and $\mathbf{J}_{22} = \mathbf{I}_M \otimes \mathbf{J}_{2M_2}$. The selection matrices for $\theta_{kl}(l = 3, 4)$ of the NC signals can also be expressed as

$$\mathbf{K}_{l1} = \text{blkdiag}\left(\mathbf{J}_{l1}, \mathbf{\Upsilon}_{(N_l-1)N}\mathbf{J}_{l2}\mathbf{\Upsilon}_{NM}\right), l = 3, 4 \tag{14}$$

$$\mathbf{K}_{l2} = \text{blkdiag}\left(\mathbf{J}_{l2}, \mathbf{\Upsilon}_{(N_l-1)N}\mathbf{J}_{l1}\mathbf{\Upsilon}_{NM}\right), l = 3, 4 \tag{15}$$

where $\mathbf{J}_{31} = \mathbf{J}_{1N_1} \otimes \mathbf{I}_N$, $\mathbf{J}_{32} = \mathbf{J}_{2N_1} \otimes \mathbf{I}_N$, $\mathbf{J}_{41} = \mathbf{J}_{1N_2} \otimes \mathbf{I}_N$ and $\mathbf{J}_{42} = \mathbf{J}_{2N_2} \otimes \mathbf{I}_N$.

Following the principle of the NC ESPRIT algorithm [21], the overdetermined set of real-valued shift invariance equations related to $\theta_{kl}(l = 1, 2, 3, 4)$ is given by

$$\tilde{\mathbf{K}}_{l1}\mathbf{E}_S\mathbf{G}_l \approx \tilde{\mathbf{K}}_{l2}\mathbf{E}_S, l = 1, 2, 3, 4 \tag{16}$$

where

$$\begin{cases} \tilde{\mathbf{K}}_{l1} = 2 \cdot \text{Re}\{\mathbf{Q}^H_{2(M_l-1)}\mathbf{K}_{l1}\mathbf{Q}^H_{2MN}\}, l = 1, 2 \\ \tilde{\mathbf{K}}_{l1} = 2 \cdot \text{Re}\{\mathbf{Q}^H_{2(N_l-1)}\mathbf{K}_{l1}\mathbf{Q}^H_{2MN}\}, l = 3, 4 \end{cases} \tag{17}$$

$$\begin{cases} \tilde{\mathbf{K}}_{l2} = 2 \cdot \text{Im}\{\mathbf{Q}^H_{2(M_l-1)}\mathbf{K}_{l1}\mathbf{Q}^H_{2MN}\}, l = 1, 2 \\ \tilde{\mathbf{K}}_{l2} = 2 \cdot \text{Im}\{\mathbf{Q}^H_{2(N_l-1)}\mathbf{K}_{l1}\mathbf{Q}^H_{2MN}\}, l = 3, 4 \end{cases} \tag{18}$$

And, the least squares (LS) principle is adopted for getting the unknown real-valued diagonal matrices $\mathbf{G}_l$, i.e.,

$$\mathbf{G}_l = (\tilde{\mathbf{K}}_{l1}\mathbf{E}_S)^+\tilde{\mathbf{K}}_{l2}\mathbf{E}_S = \mathbf{E}\mathbf{\Theta_l}\mathbf{E}^{-T}, l = 1, 2, 3, 4 \tag{19}$$

where

$$\mathbf{\Theta}_l = \text{diag}\left(\tan\left(\frac{2\pi\lambda^{-1}d\cos\theta_{1l}}{2}\right), \cdots, \tan\left(\frac{2\pi\lambda^{-1}d\cos\theta_{Kl}}{2}\right)\right) \tag{20}$$

are diagonal matrices, and $\mathbf{E}$ is the $K \times K$ unitary matrix. Because $\mathbf{\Theta}_{kl}(l = 1, 2, 3, 4)$ are real values, we first select any two different real-valued diagonal matrices $\mathbf{G}_i$ and $\mathbf{G}_j$, and then use the complex decomposition [11] to achieve automatically paired angle estimates θ_i and θ_j as follows

$$\mathbf{G}_i + j\mathbf{G}_j = \mathbf{E}\{\mathbf{\Theta}_i + j\mathbf{\Theta}_j\}\mathbf{E}^{-1}, i \in l, j \in l, i \neq j \tag{21}$$

Then the paired estimate of θ_i and θ_j can be obtained by extracting the real and imaginary parts of the feature eigenvalues $\mathbf{\Theta}_i + j\mathbf{\Theta}_j$:

$$\begin{cases} \hat{\theta}_{ki} = \arccos\left(\lambda \arctan(\mathbf{\Theta}_{ki})/(\pi d)\right) \\ \hat{\theta}_{kj} = \arccos\left(\lambda \arctan(\mathbf{\Theta}_{kj})/(\pi d)\right) \\ \quad k = 1, 2, \cdots, K, \;\; l = 1, 2, 3, 4, \;\; i \in l, \; j \in l, \; i \neq j \end{cases}, \tag{22}$$

In order to pair the four angles, we need to perform at least three pairing operations with two different angles according to Eqs. (21) and (22).

Till now, the proposed method provides closed-form 2D-DOA and 2D-DOD angle estimates, which are automatically paired, and is summarized in Table 1.

Remark 1: The major computational effort of the proposed algorithm contains performing SVD of $\hat{\mathbf{Z}}$ and the implementation of unitary ESPRIT algorithm. SVD of $\hat{\mathbf{Z}}$ requires the amount of complex multiplications of $O((2MN)^3)$. Owing to real valued processing, the computational cost of the unitary ESPRIT algorithm is a quarter of that of the conventional ESPRIT algorithm, which further reduces the computational complexity.

Remark 2: The maximum number of detectable signals by the proposed algorithm is based on the new data vector in Eq. (4) as well as the matrices K_{l1} and K_{l2}, $l = 1$, 2 in Eqs. (12) and (13) for 2D DODs, K_{l1} and K_{l2}, $l = 3$, 4 in Eqs. (14) and (15) for 2D DOAs. The maximum detectable signal number of our proposed algorithm is $\begin{cases} K_{DOD} = \min\{2N(M_1 - 1), 2N(M_2 - 1)\} \\ K_{DOA} = \min\{2M(N_1 - 1), 2N(N_2 - 1)\} \end{cases}$.

Table 1. Summary of the proposed algorithm.

Step 1 Define a new data matrix $\mathbf{Y}$, and obtain the real-valued matrix $\mathbf{Z}$.
Step 2 Perform SVD on $\hat{\mathbf{Z}}$ to get $\hat{\mathbf{U}}_S$, and then compute $\hat{\mathbf{E}}_S = \hat{\mathbf{U}}_S\hat{\mathbf{\Sigma}}_S$.
Step 3 Construct the rotational invariant equation (16), then solve them by means of LS to obtain rotational factor matrices $\mathbf{G}_l$.
Step 4 Pair the elements of $\mathbf{G}_l$ according to (21).
Step 5 Compute $\hat{\theta}_{kl}$ according to (22).

4. CRAMER-RAO BOUND

In this section, the deterministic NC CRB for the estimates of 2D-DOA and 2D-DOA is derived for the L-shaped bistatic MIMO radar.

Under the deterministic assumption, $\mathbf{Y}$ are circularly Gaussian distributed with mean $\mathbf{C}_e\mathbf{S}(t)$ and covariance $\sigma^2\mathbf{I}_{2MN}$, where $\mathbf{C}_e = [\mathbf{C}^T, \mathbf{C}^H\mathbf{\Phi}^T]^T$. According to [22], the $5K \times 5K$ CRB matrix of $\theta_{kl}(l = 1, 2, 3, 4)$ and φ_k is given by

$$\text{CRB} = \frac{L}{\sigma^2}\left\{\text{Re}\left[\mathbf{D}^H\mathbf{P}_{\mathbf{C}_e}^{\perp}\mathbf{D} \odot \mathbf{R}\right]\right\}^{-1} \tag{23}$$

where $\mathbf{P}_{\mathbf{C}_e}^{\perp} = \mathbf{I}_{2MN} - \mathbf{C}_e(\mathbf{C}_e^H\mathbf{C}_e)^{-1}\mathbf{C}_e^H$, $\mathbf{R}$=$\mathbf{1}_5 \otimes \mathbf{1}_5^T \otimes \mathbf{R}_S^T$ and $\mathbf{R}_S$ is the covariance matrix of $\mathbf{S}(t)$. $\mathbf{D} = [\mathbf{D}_1, \mathbf{D}_2, \mathbf{D}_3, \mathbf{D}_4, \mathbf{D}_5]$ with $\mathbf{D}_l = \left[\frac{\partial \mathbf{C}_e}{\partial \theta_{1l}}, \cdots, \frac{\partial \mathbf{C}_e}{\partial \theta_{Kl}}\right]$ $(l = 1, 2, 3, 4)$, $\mathbf{D}_5 = \left[\frac{\partial \mathbf{C}_e}{\partial \varphi_1}, \cdots, \frac{\partial \mathbf{C}_e}{\partial \varphi_K}\right]$.

5. SIMULATION RESULTS

In this section, the proposed algorithm is compared with the ESPRIT algorithm [9], Xia's algorithm [14], the deterministic CRB in [14], and the derived NC deterministic CRB. The first experiment is based on an L-shaped MIMO array with $M_1 = M_2 = N_1 = N_2 = 2$ and for the next experiment, $M_1 = M_2 = N_1 = N_2 = 3$, and d is the half wavelength. We use the root mean square error (RMSE) given by

$\text{RMSE\_DOD} = \sqrt{\frac{1}{KM_c}\sum_{k=1}^{K}\sum_{m=1}^{M_c}\left[\left(\hat{\theta}_{k1} - \theta_{k1}\right)^2 + \left(\hat{\theta}_{k2} - \theta_{k2}\right)^2\right]}$ and

$\text{RMSE\_DOA} = \sqrt{\frac{1}{KM_c}\sum_{k=1}^{K}\sum_{m=1}^{M_c}\left[\left(\hat{\theta}_{k3} - \theta_{k3}\right)^2 + \left(\hat{\theta}_{k4} - \theta_{k4}\right)^2\right]}$ as the performance criterion, where M_c is the number of Monte-Carlo trials.

Experiment 1. In the first experiment, we verify that the proposed method can increase the number of maximum detectable signals, as compared to other methods. We consider five uncorrelated NC signals with direction pairs $(60°, 105°, 60°, 105°)$, $(70°, 80°, 70°, 80°)$, $(85°, 90°, 85°, 90°)$, $(100°, 70°, 100°, 70°)$ and $(110°, 100°, 110°, 100°)$. The number of snapshots is 300, and the SNR is set at 20dB and $M_c = 100$. Fig. 2 shows the 2D-DODs and 2D-DOAs scattergram of five NC signals, respectively. It can be seen that the proposed algorithm can estimate the 2D-DODs and 2D-DOAs of five NC signals correctly with available noncircular information, while the algorithm in [9] and [14] fail to work.

Experiment 2. In the second experiment, we consider the scattergrams of four closely spaced NC signals distinguished by the proposed algorithm and other algorithms. The four NC signals are from direction pairs $(65°, 70°, 65°, 70°)$, $(65°, 65°, 65°, 65°)$, $(70°, 65°, 70°, 65°)$ and $(70°, 70°, 70°, 70°)$. The number of snapshots is 1000, the SNR set at 25 dB, and $M_c = 100$. Figs. 3(a) and (b) show the 2D-DODs and 2D-DOAs scattergrams of four NC signals, respectively. As shown in Fig. 3, the 2D-DOA and 2D-DOD of the proposed algorithm are slightly scattered for the cases of closely spaced sources, but the estimated angles are roughly distributed around the true values. However, the algorithms in [9] and [14] fail to work.

Experiment 3. In the third experiment, the performance of the proposed algorithm is studied with SNR varying from -5 dB to 15 dB. We consider four uncorrelated NC signals with direction pairs $(60°, 40°, 70°, 50°)$, $(70°, 50°, 80°, 70°)$, $(80°, 60°, 90°, 80°)$ and $(100°, 70°, 100°, 90°)$. The number of snapshots is 300 and $M_c = 2000$. As shown in Fig. 4, the estimation performance of the proposed algorithm is shown to be superior to ESPRIT algorithm [9] and Xia's algorithm [14] for both 2D-DOD and 2D-DOA estimations by utilizing the noncircular information. In addition, the CRB using NC signals is better, and the estimated performance of the proposed algorithm is even better than CRB without using noncircular information.

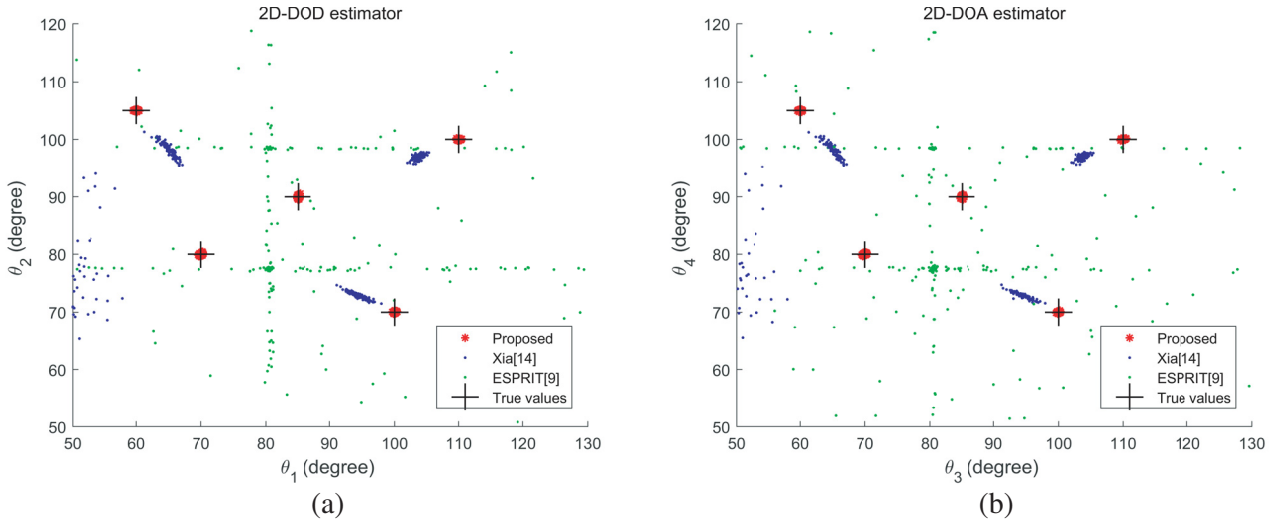

Figure 2. 2D-DOD and 2D-DOA scattergrams of five NC signals. (a) 2D-DOD estimator. (b) 2D-DOA estimator.

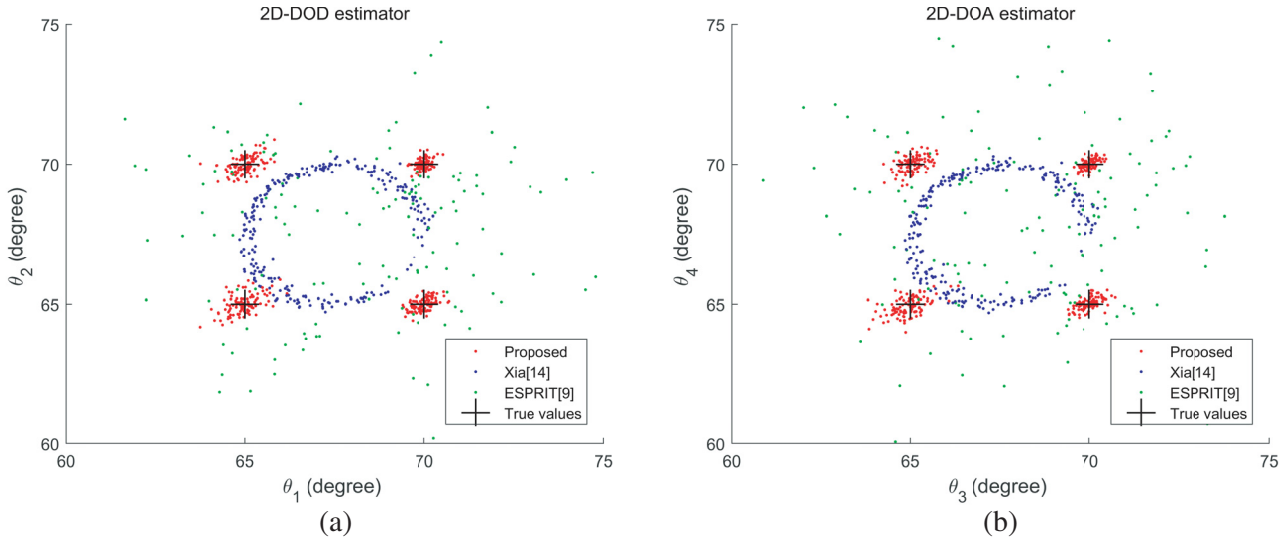

Figure 3. 2D-DOD and 2D-DOA scattergrams of four closely spaced NC signals. (a) 2D-DOD estimator. (b) 2D-DOA estimator.

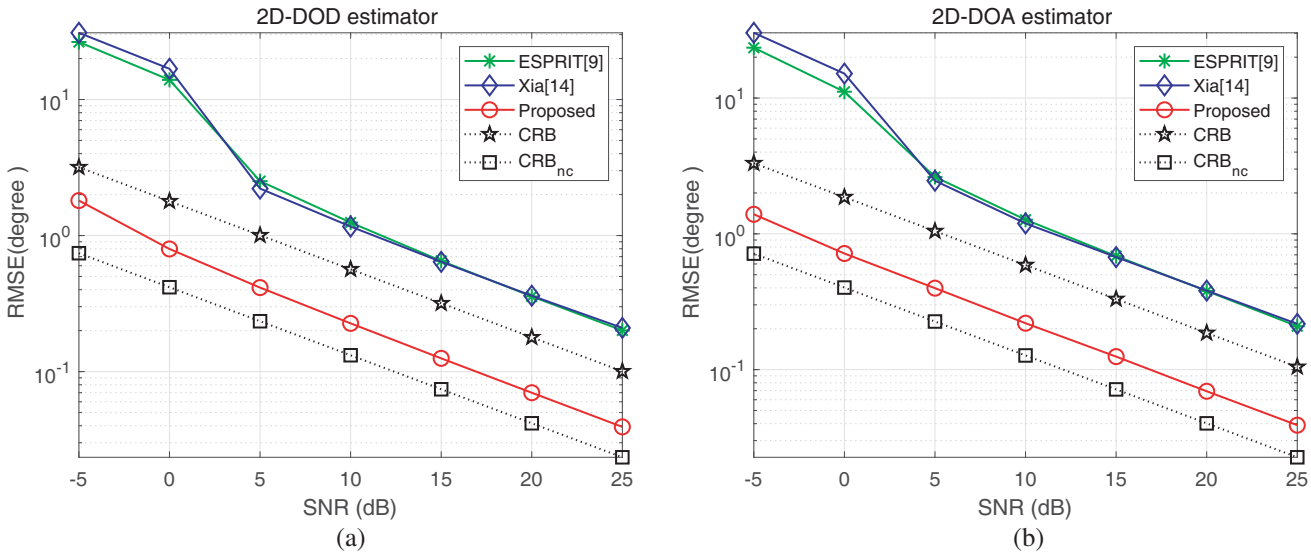

Figure 4. RMSE of 2D-DOA for NC signals versus SNR. (a) 2D-DOD estimator. (b) 2D-DOA estimator.

6. CONCLUSION

Based on the unitary ESPRIT, NC-based 2D-DOD and 2D-DOA estimation algorithm for L-shaped bistatic MIMO radar is proposed in this paper. It utilizes the noncircularity characteristic to construct a virtual array and then derives the NC unitary ESPRIT algorithm to achieve automatically paired 4D angles of NC signals. The NC deterministic CRB is also analyzed. Simulation results show that the proposed algorithm has better angle estimation performance than the algorithm without noncircularity characteristics. Finally, we will consider further research from the following two aspects: 1. Whether the proposed algorithm is applicable in the case of mixed noncircular and circular signals. 2. Whether the proposed algorithm is applicable in the case of noncircular distributed sources.

ACKNOWLEDGMENT

This work is supported by Key Laboratory of Intelligent Perception and Advanced Control of State Ethnic Affairs Commission under Grant MD-IPAC-2019102, and by Zhejiang Provincial Natural Science Foundation of China under Grant LQ19F010002, and by Natural Science Foundation of Ningbo Municipality under Grant 2018A610094, and by K. C. Wong Magna Fund in Ningbo University.

REFERENCES

1. Chen, H., X. Zhang, Y. Bai, and J. Ma, "Direction finding for bistatic MIMO radar with non-circular sources," *Progress In Electromagnetics Research M*, Vol. 66, 173–182, 2018.
2. Chintagunta, S. and P. Ponnusamy, "Spatial and polarization angle estimation of mixed-targets in MIMO radar," *Progress In Electromagnetics Research M*, Vol. 82, 49–59, 2019.
3. Wen, F., J. Shi, and Z. Zhang, "Joint 2D-DOD, 2D-DOA, and polarization angles estimation for bistatic EMVS-MIMO radar via PARAFAC analysis," *IEEE Transactions on Vehicular Technology*, Vol. 69, No. 2, 1626–1638, Feb. 2020.
4. Liu, S., J. Zhao, Z. Yuan, R. Zhou, M. Xiao, and C. Lu, "Localization for mixed near-field and far-field sources by interlaced nested array," *Progress In Electromagnetics Research M*, Vol. 82, 107–115, 2019.

5. Ciuonzo, D., G. Romano, and R. Solimene, "Performance analysis of time-reversal MUSIC," *IEEE Trans. on Signal Process.*, Vol. 63, No. 10, 2650–2662, May 2015.
6. Ciuonzo, D. and P. S. Rossi, "Noncolocated time-reversal MUSIC: High-SNR distribution of null spectrum," *IEEE Signal Process. Lett.*, Vol. 24, No. 4, 397–401, Apr. 2017.
7. Ciuonzo, D., "On time-reversal imaging by statistical testing," *IEEE Signal Process. Lett.*, Vol. 24, No. 7, 1024–1028, Jul. 2017.
8. Zhang, X., L. Xu, L. Xu, and D. Xu, "Direction of departure (DOD) and direction of arrival (DOA) estimation in MIMO radar with reduced-dimension MUSIC," *IEEE Communications Letters*, Vol. 14, No. 12, 1161–1163, Dec. 2010.
9. Duofang, C., C. Baixiao, and Q. Guodong, "Angle estimation using ESPRIT in MIMO radar," *Electron. Lett.*, Vol. 44, No. 12, 770–771, Jun. 2008.
10. Xia, T. Q., "Joint diagonalization based DOD and DOA estimation for bistatic MIMO radar," *Signal Process.*, Vol. 108, 159–166, 2015.
11. Zheng, G. M. and B. X. Chen, "Unitary dual-resolution ESPRIT for joint DOD and DOA estimation in bistatic MIMO radar," *Multidimensional Systems and Signal Processing*, Vol. 26, No. 1, 159–178, 2015.
12. Bencheikh, M. L. and Y. Wang, "Joint DOD-DOA estimation using combined ESPRIT-MUSIC approach in MIMO radar," *Electronics Letters*, Vol. 46, No. 15, 1081–1083, Jul. 2010.
13. Zheng, Z. D., J. Zhang, and J. Y. Zhang, "Joint DOD and DOA estimation of bistatic MIMO radar in the presence of unknown mutual coupling," *Signal Process.*, Vol. 92, No. 12, 3039–3048, Dec. 2012.
14. Xia, T. Q., "Joint diagonalization based 2D-DOD and 2D-DOA estimation for bistatic MIMO radar," *Signal Process.*, Vol. 116, 7–12, 2015.
15. Xu, L. Y., X. F. Zhang, Z. Z. Xu, X. W. Zeng, and F. Q. Yao, "Joint Doppler frequency, 2D-DOD and 2D-DOA estimation for bistatic MIMO radar in spatial coloured noise," *IEEE Trans. on Signal Process.*, Vol. 102, 1007–1021, 2015.
16. Chen, H., W. Liu, W. P. Zhu, M. N. S. Swamy, and Q. Wang, "Mixed rectilinear sources localization under unknown mutual coupling," *Journal of The Franklin Institute (Elsevier)*, Vol. 356, No. 4, 2372–2394, 2019.
17. Abeida, H. and J. P. Delmas, "Direct derivation of the stochastic CRB of DOA estimation for rectilinear source," *IEEE Signal Process. Lett.*, Vol. 24, No. 10, 1522–1526, Oct. 2017.
18. Bencheikh, M. L. and Y. Wang, "Non circular ESPRIT-Root MUSIC joint DOA-DOD estimation in bistatic MIMO radar," *International Workshop on Systems, Signal Processing and Their Applications*, 9–11, 2011.
19. Zheng, G. M., J. Tang, and X. Yang, "ESPRIT and unitary ESPRIT algorithms for coexistence of circular and noncircular signals in bistatic MIMO radar," *IEEE Access.*, Vol. 4, 7232–7240, 2016.
20. Guo, Y. D., Y. S. Zhang, J. Gong, and G. M. Zheng, "Direction finding with real-valued ESPRIT for noncircular signal in bistatic MIMO radar," *Wireless Personal Communications*, Vol. 95, No. 3, 3321–3332, 2017.
21. Chen, H., C. P. Hou, W. P. Zhu, W. Liu, Y. Y. Dong, Z. J. Peng, and Q. Wang, "ESPRIT-like two-dimensional direction finding for mixed circular and strictly noncircular sources based on joint diagonalization," *Signal Processing*, Vol. 141, 48–56, 2017.
22. Chen, H., W. F. Wang, and W. Liu, "Joint DOA, range, and polarization estimation for rectilinear sources with a COLD array," *IEEE Wireless Communications Letters*, Vol. 8, No. 5, 1398–1401, Sept. 2019.